Microstructure, hardness and petroleum corrosion evaluation of 316L/AWS E309MoL-16 weld metal

Cleiton C. Silva[a,*], *Hélio C. de Miranda*[a], *Hosiberto B. de Sant'Ana*[b], *Jesualdo P. Farias*[a]

[a]*Universidade Federal do Ceará, Department of Materials and Metallurgical Engineering, Fortaleza, Ceará, Brazil*
[b]*Universidade Federal do Ceará, Department of Chemical Engineering, Fortaleza, Ceará, Brazil*

ARTICLE DATA

Article history:
Received 22 January 2008
Received in revised form
25 September 2008
Accepted 29 September 2008

Keywords:
Stainless steel
Weld metal
δ-Ferrite
Microstructure
Corrosion

ABSTRACT

The current work presents some observations about the effect of welding heat input on the microstructure, hardness and corrosion resistance of AWS E309MoL-16 weld metal, diluted with AISI 316L austenitic stainless steel plates. Such welds are widely used during overlay of equipment in the petroleum and gas industries. Results show that the welds contained δ-ferrite varying between vermicular to lathy morphology, typically encountered in welds which solidify in ferrite–austenite mode (FA). Conversely, contents and morphology of δ-ferrite in the weld metals were altered, showing an increase of welding heat input. The corrosion rate of the weld metal indicated that when higher levels of welding heat input are used the corrosion rate is reduced. This may be attributed to metallurgical changes, especially variations in the proportion of δ-ferrite, caused by changes in cooling rate.

1. Introduction

Austenite stainless steel consumables are widely used in the welding of stainless steel. Typical cooling rates during welding are quite rapid, leading to non-solidification. Such sudden drop to room temperature may result in a microstructure consisting of ferrite and austenite, depending on the chemical composition of the join. In the later case, the ferrite present is usually δ-ferrite formed at high temperatures [1,2].

Several researchers have dedicated themselves to the study of solidification and classification of the microstructure resulting in stainless steel weld metals [3–6]. Their research has made available essential results for the understanding of solidification mechanisms and solid states transformations, as well as data relating chemical composition to phase percentages, solidification form and microstructural morphology.

Several diagrams have been developed to predict the microstructure in the welding of similar and dissimilar metals [7–9]. They also relate various alloy elements in the weld metal that have a remarkable influence on the microstructure. These diagrams are based on two equations. The first one is the chromium equivalent equation (Cr_{eq}) that involves the ferritizing elements. The second one is the nickel equivalent equation (Ni_{eq}) which involves elements that stabilize the austenite phase. These equations, and the correspondent diagram WRC-1992 (Welding Research Council) developed by Kotecki and Siewert [9] are shown below.

$$Cr_{eq} = \%Cr + \%Mo + 0.7\,Nb \quad (1)$$

$$Ni_{eq} = \%Ni + 35(\%C) + 20(\%N) + 0.25(\%Cu) \quad (2)$$

Stainless steel with a Cr_{eq}/Ni_{eq} ratio below 1.2 solidifies in the primary austenite mode. In this mode, initially nucleation of austenite occurs in the liquid metal. As austenite grains grow ferritizing elements are segregated to the liquid, which may solidify as austenite or some δ-ferrite, depending on the level of ferrite promoting elements present in the liquid.

For Cr_{eq}/Ni_{eq} ratios between 1.2 and 1.5, the chemical composition of the liquid becomes favorable for the

* *Corresponding author*. Tel.: +55 85 33669358; fax: +55 85 33669969.
E-mail address: cleitonufc@yahoo.com.br (C.C. Silva).

1044-5803/$ – see front matter © 2008 Elsevier Inc. All rights reserved.
doi:10.1016/j.matchar.2008.09.017

formation of δ-ferrite. Such microstructure is characteristic in the AF (austenite–ferrite) solidification mode. Should the chemical composition of the liquid not be sufficiently rich in ferritizing elements to promote the formation of δ-ferrite, solidification will entirely result in predominant austenitic microstructure (A).

The inconvenience of such solidification mode would reflect on the impurity segregation of elements such as phosphorous and sulphur in the remaining liquid. Additionally, the formation of low-melting-point compounds responsible for hot cracking usually occurs [1,10,11]. According to the literature, welds should contain some percentage of δ-ferrite at room temperature to ensure that noxious elements segregated during the solidification are retained by it, thus reducing hot cracking [11–13].

Influence of the chemical composition of the microstructure in austenitic stainless steel weld metals is well understood, being usually the only variable used to predict microstructure. However, other variables may also influence microstructural characteristics of weld metals, such as the cooling rate.

In the petroleum, gas and petrochemical industries AWS E309MoL-16 electrodes are frequently utilized for both linings and overlay applications. In these cases, dilution represents the main factor evaluated to predict microstructure, even though it usually constitutes a parameter often difficult to determine. In addition, ranges of welding parameters that can be used under these circumstances are often wide, generating alterations in the cooling rate of the weld. As a result, significant microstructural alterations could be obtained and thus influence mechanical properties and corrosion resistance. Under such perspective, the present study compiles observations regarding the effect of welding heat input on the microstructure, hardness and corrosion resistance of AWS E309MoL-16 austenitic stainless steel weld metal, diluted in AISI 316L austenitic stainless steel plates.

2. Materials

The base metal selected for the study was AISI 316L austenitic stainless steel, with a chemical composition shown in Table 1. AWS E309MoL-16 austenitic stainless steel covered electrodes with a diameter of 2.5 mm were selected as the filler metal for the experiments. The chemical composition of the filler metal, according to the manufacturer, is presented in Table 2.

Welding was performed in the plane position on AISI 316L stainless steel plate samples, with dimensions of 50×150×3 mm. Shielding metal arc welding (SMAW) was the technique implemented during the tests. Three weld beads were deposited on each plate, beside each other to form a layer. This procedure was performed manually, with control over the welding speed. A multi-process INVERSAL 450 welding source and a data acquisition system (arc current and voltage) was used. Three levels of welding heat input were used in this task. Specific parameters are shown in Table 3. The interpass temperature was maintained at 150 °C to avoid variations in the cooling rate among the passes.

Table 1 – Chemical composition of the AISI 316L austenitic stainless steel (weight %)

C	Mn	Cr	P	S	Mo	Si	Ni	N
0.022	1.36	16.93	0.03	0.003	2.09	0.47	10.11	411[a]

[a] Value in ppm.

Table 2 – Chemical composition of the AWS E309MoL-16 austenitic stainless steel weld metal (weight %)

C	Cr	Ni	Mo
0.03	23	13	2.5

Metallographic specimens were prepared conventionally through sandpaper and polishing using diamond paste. Etching was carried out using Vilela's reagent (100 mL of ethylic alcohol + 1 g of picric acid and + 5 mL of chloridric acid). For the metallographic analysis the following techniques were used: an optical microscope (OM), a Scanning Electron Microscope (SEM), and an energy dispersive X-ray spectroscopy (EDS). The level of ferrite δ was determined by means of an optical microscopy using the *Image Pro Plus* image analyzer, and through magnetic analysis using a ferritoscope. It should be noticed that each specimen was analyzed with 40 fields of view per data with a magnification of 200×. Vickers Microhardness measurements were also carried out with a load charge of 1 N (0.1 kgf) on each the welded specimen, with an average of 20 tests per specimen at random, and 20 tests for each morphology.

Corrosion tests on weld metal specimens at high temperature (300 °C), and immersed on heavy petroleum for 60 h. Brazilian heavy petroleum (from Campos Basin), kindly supplied by Centro de Pesquisas e Desenvolvimento Leopoldo Américo M. de Mello — CENPES/PETROBRAS, was utilized in the analysis. It is important to note, that the petroleum was not previously treated for the tests. Density, oil viscosity, and sulfur content in the sample were determined. Results of these analyses are shown in Table 4. Upon completion of the experiment, specimens were cleaned in kerosene for subsequent evaluation of their surface, using a SEM and the energy dispersive X-ray spectroscopy test. Corrosion rates in the samples were determined through Eq. (3) shown below, following ASTM G1 standard [14].

$$\text{Corrosion rate (mm/year)} = (K \times DM)/(S \times t \times q) \quad (3)$$

Where:

K constant ((mm h)/(year cm)) – 8.76×10^4;
ΔM mass loss in grams;

Table 3 – Welding parameters

Current (A)	Voltage (V)	Welding speed (cm/min)	Welding heat input (kJ/cm)
80	25	20.0	6.0
80	25	12.5	9.6
80	26	10.0	12.4

Table 4 – Petroleum characterization

Density (20/40)	API°	Viscosity 50 °C (mm^2/s)	Sulfur content (%m/m)
0.91042	16.8	240	0.56

S coupon exposed area in cm^2;
t time of exposure in hours;
ρ specific mass of the steel (g/cm^3).

3. Results and Discussions

3.1. *Dilution Evaluation and δ-ferrite Content*

AWS E309MoL-16 weld metals deposited on 316L plates presented a microstructure constituted primarily by austenite and δ-ferrite. The three welding heat inputs (6 kJ/cm, 9 kJ/cm, and 12 kJ/cm) implemented resulted in three levels of dilution of 32, 34, and 37%, respectively.

Values for Cr_{eq} and Ni_{eq} were calculated using the dilution results obtained for each welds and are presented in Table 5. In these results, it is possible to observe that values for Ni_{eq} remain constant, regardless of the dilution. It is inferred that such behavior can be found since both, the base metal (AISI 316L) and the weld metal (AWS E309MoL) have equal values of Ni_{eq}. The Cr_{eq} values slightly varied, presumably due to its low level of dilution. In all three cases, the Cr_{eq}/Ni_{eq} ratio indicated that the solidification mode was ferrite–austenite (FA).

Although variation in the chemical composition of the weld metal was not significant (Table 4), δ-ferrite content measured in the three welding conditions presented variations. As it can be observed in Fig. 1, levels of δ-ferrite tend to decrease with an increase in welding heat input, regardless of the measurement technique employed (ferritoscope or image analysis). In this case, reductions in the level of δ-ferrite have been attributed to a slower cooling rate when the welding heat input is increased. This assumption is based on the theory that the cooling rate has a significant influence on solidification and solid state transformations of stainless steel weld metals, especially for levels of δ-ferrite above 14% [15].

Slower cooling rates would translate into welds that remain longer in the $\delta \rightarrow \gamma$ transformation temperature range, thus causing a greater percentage of δ-ferrite to be transformed into austenite. Consequently, a smaller volumetric fraction of the δ-ferrite phase in the weld metal at room temperature would be obtained.

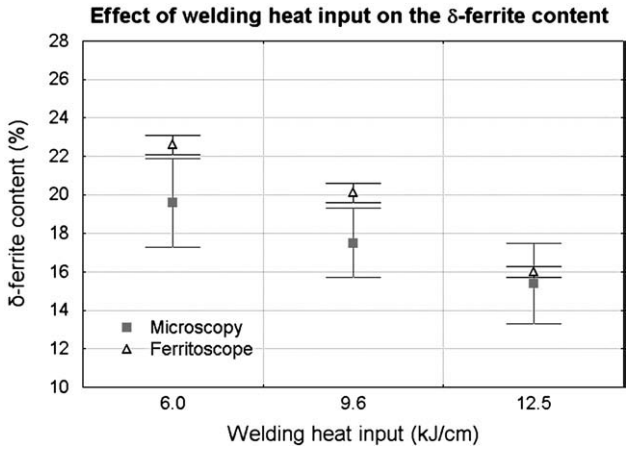

Fig. 1 – Welding heat input effect on the δ-ferrite.

Elmer et al. [16], state that when solidification of the weld metal occurs in the primary austenite mode (AF), an increase in the cooling rate contributes towards the formation of austenite. This would also generate a reduction in the amount of segregated solute during the solidification, which ultimately reduces the formation of δ-ferrite as a secondary phase. However, when solidification occurs in the primary ferrite phase (FA) or is completely ferritic (F), the increase in the cooling rate leads to an increase in the δ-ferrite levels. This is due to an increase in the original δ-ferrite level from the solidified liquid metal, and a reduction in the ferrite–austenite solid state transformation.

3.2. *δ-Ferrite Morphology Evaluation*

The morphology of δ-ferrite was also altered with variation of welding heat input. Fig. 2a, b and c shows the correspondent microstructures of the weld metals for 6, 9 and 12 kJ/cm welding heat input, respectively.

After the evaluation of the microstructure, weld metals exposed to the lowest heat input (6 kJ/cm) had predominantly δ-ferrite lathy morphology, characteristic in both ferrite–austenite (FA) and completely ferritic (F) weld metal solidification mode [5,6,17,18]. It also presented higher levels of δ-ferrite (Fig. 2a). Welds tested at 9 kJ/cm had a similar microstructure to the previous set of results. Nonetheless, less lathy δ-ferrite (Fig. 2b) and little δ-ferrite with vermicular morphology were detected. Finally, samples at 12 kJ/cm presented microstructure of δ-ferrite in vermicular form, as can be observed in Fig. 2c. Vermicular morphology is typical of welds that solidify

Table 5 – Results of the dilution, Creq/Nieq and δ-ferrite analysis

Welding heat input (kJ/cm)	Dilution (%)	Cr_{eq}	Ni_{eq}	Cr_{eq}/Ni_{eq}	δ-Ferrite (%)	
					Microscopy	Ferritoscope
6.0	32	23.6	14.1	1.67	19.6±2.3	22.6±0.5
9.6	34	23.5	14.1	1.67	17.5±1.8	20.1±0.5
12.4	37	23.3	14.1	1.65	15.4±2.1	16.0±0.3

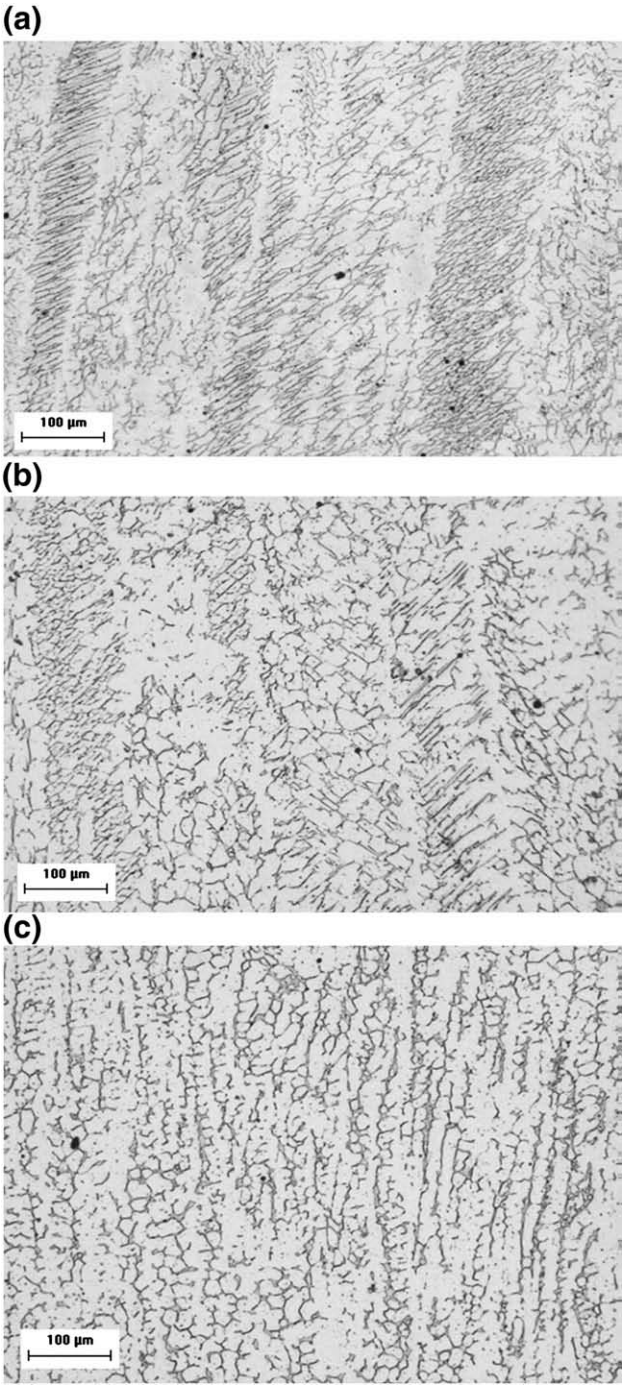

Fig. 2 – Weld metal microstructure. (a) 6 kJ/cm; (b) 9 kJ/cm; (c) 12 kJ/cm. Enlarged: 200×. Etching: Vilela.

in the ferrite–austenite (FA) or ferrite (F) mode and have usually low levels of δ-ferrite [1,19].

Vermicular and lathy morphologies are observed in the welds that solidified in FA and F region of the pseudo-binary diagram. Several authors argue that such microstructure formation mechanism depends on variations in the chemical composition during the cooling of the weld. Suutala et al. [20] state that the sequence for the formation of weld metal occurs firstly with the initial solidification of the liquid metal in ferrite, followed by a subsequent formation of austenite involving the grains of ferrite until the complete solidification. They suggest that much of the ferrite resulting from the solidification is transformed into austenite by a solid state transformation process controlled by diffusion. Brooks et al. [21] studied the origin of vermicular morphology, which they call skeletal ferrite morphology. Using transmission electron microscopy they proved that during cooling transformations there is a separation of chrome to ferrite and nickel to austenite. They also showed that lathy ferrite occurs through the same process of controlled diffusion.

3.3. *Microhardness Evaluation*

Microhardness analysis, presented in Fig. 3, shows that the hardness had a tendency to decrease with increases in heat input. Such behavior can be attributed to two main factors. The first, is the reduction in the level of δ-ferrite with increases in welding heat input, which indicate that the greater the level of δ-ferrite the harder the solder. The second factor is represented by the morphology of δ-ferrite. The last two values shown in Fig. 3 are hardness values related to lathy and vermicular morphology, respectively. These data show that the average hardness of lathy δ-ferrite morphology is superior to the average value of vermicular δ-ferrite morphology. Although the morphologies are intrinsically related to the level of δ-ferrite, their effect should not be disregarded.

Padilha and Guedes [22], cite the increase in the volumetric fraction of δ-ferrite leading to higher levels of hardness. Cardoso et al. [23] studied the influence of the shielding gas on the characteristics of E309 welds. They also verified variations in hardness, which were attributed to the δ-ferrite levels present in the weld metals, maintaining the same ratio of increase in hardness for greater volumetric fractions of the correspondent phase.

3.4. *Corroded Surface Characterization*

Evaluation of the weld metals' surface is presented in Fig. 4. Specimens welded with 6 kJ/cm of heat input presented the highest levels of corrosion as it can be observed in Fig. 4a.

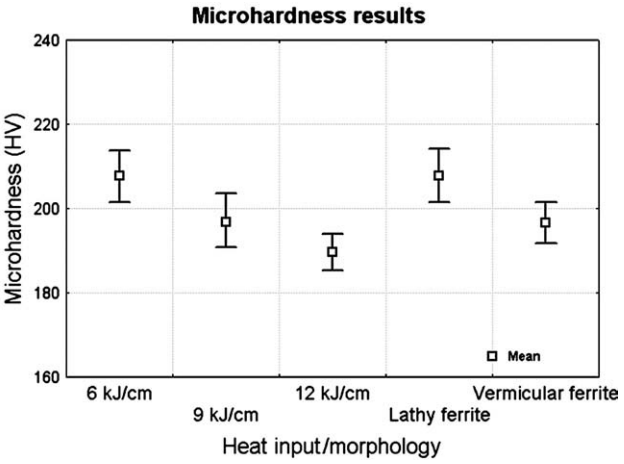

Fig. 3 – Vickers microhardness values.

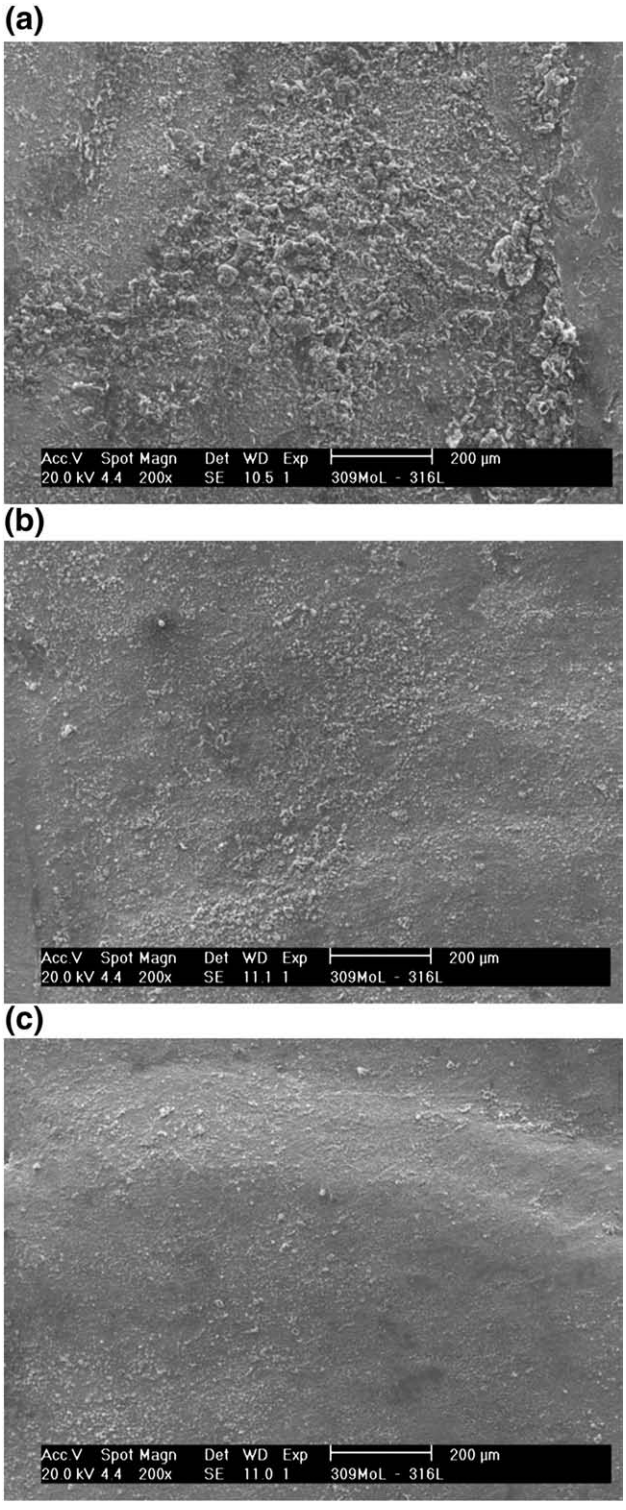

Fig. 4 – Weld metal surface after corrosion trails. (a) 6 kJ/cm. (b) 9 kJ/cm. (c) 12 kJ/cm.

Fig. 4b shows less formation of the corrosion product, which may indicate a less intense attack when compared to 6 kJ/cm tested samples. Specimens on which the greatest welding heat input was used (12 kJ/cm), presented the least intense attack (Fig. 4c), but even so it was totally covered by a layer of iron sulphide, as it was indicated by EDX analysis.

Formation of iron sulphide as a corrosion product is a strong indication of corrosion processes associated to hydrogen sulphide, as well as corrosion by naphthenic acids. Corrosion processes are typically associated to high ranges of temperature, generally varying between 200 and 400 °C [24,25].

High temperature hydrogen-sulphide corrosion (HTHC) occurs due to the presence of hydrogen sulphide above 260 °C, and is characteristic of equipment in refineries which process crude petroleum with high levels of sulphur [24,25]. Yet, corrosion caused by naphthenic acids is more complex, and there is no clear distinction between the damage caused by naphthenic acids and corrosion by hydrogen sulphide.

Three factors should be considered when determining potential naphthenic corrosion. Naphthenic petroleum acids presence can be determined by various methods. Total Acid Number (TAN), which expresses the quantity of KOH in milligrams needed to neutralize a particular amount of oil in grams, expressed in [mg KOH/g oil] is generally the most common one. However, in many cases, quantification is mixed up leading to erroneous data. According to the literature, for TAN that exceed 0.5, samples contain enough naphthenic acid to potentially cause naphthenic corrosion. Others factors contribute to naphthenic corrosion. Among these can be cited temperature ranges to which the oil is subjected and physical aspects such as concentration and flow speed of the mixture. Usually, acceptable temperature ranges vary between 230 and 400 °C, with a maximum corrosion rate occurring at 370 °C [26–29].

The TAN selected for crude petroleum used in this study has a high level of corrosiveness, even above the minimum necessary for potential corrosion damage by naphthenic acids. The temperature used in the tests is high enough and within the range in which corrosion by naphthenic acids is likely to occur. Additionally, corrosion products observed were made up of iron sulphide, commonly found when naphthenic acid corrosion takes place. In this order of ideas, after the experiment strong indicators reinforce the theory that the major corrosion phenomenon caused by heavy oils is due indeed to naphthenic acids.

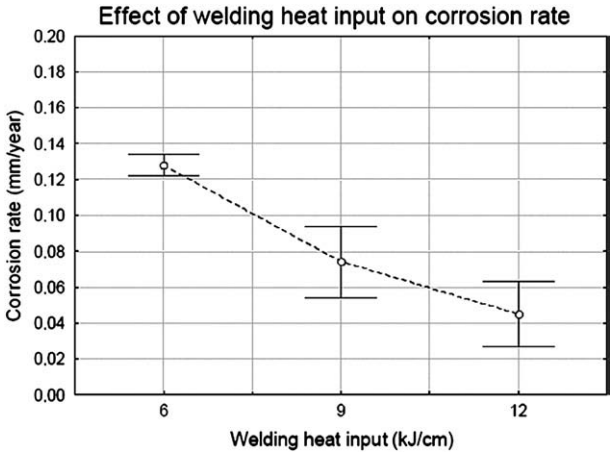

Fig. 5 – Welding heat input effect on the corrosion rate.

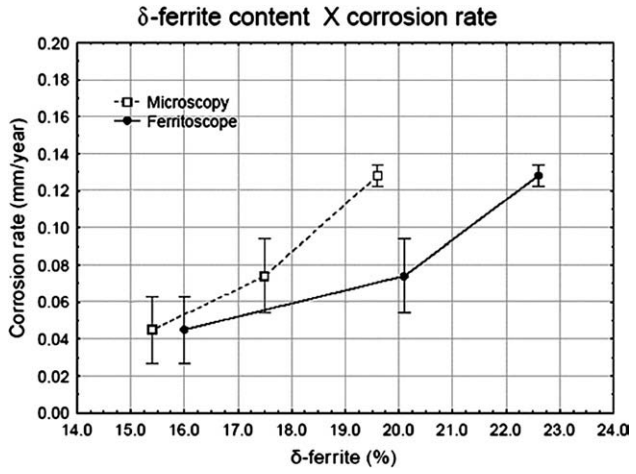

Fig. 6 – Effect of δ-ferrite content on the corrosion rate.

3.5. *Corrosion Rate Evaluation*

The corrosion rate of the weld metals for the three welding conditions is presented in Fig. 5. According to the results, the corrosion rate falls slightly with increases in welding heat input. From the point of view of dilution, the increase in welding heat input causes a slight increase in the dilution of the weld metal. However, such alteration does not cause a significant variation in the overall chemical composition. This relates to the fact that base metal and weld metal have similar chemical values, especially for nickel and molybdenum. Data in this respect is presented above in the microstructural characterization section.

When comparing corrosion rate results to microstructure, it can be seen that a reduction in the corrosion rate may result from reductions in δ-ferrite content. Welded AISI 316L specimens with the lowest welding heat input (6 kJ/cm) yielded the lowest δ-ferrite content. Thus, an increase in welding heat input could leads to reduction in the percentage of this phase. Fig. 6 shows corrosion rate results for δ-ferrite contents. Here, it can be observed that corrosion rates seem to be promoted by the increase in the percentage of δ-ferrite.

The effect of δ-ferrite on corrosion resistance can be also attributed to the difference in the chemical composition between ferrite and austenite, due to segregation during solidification. It is well known that δ-ferrite is more rich in chromium content, this fact can explain its high resistance to corrosion when compared with austenite phase. Besides of that, the presence of two phases with different corrosion resistance can form an active-passive region, accelerating the attack on the austenite matrix. This characteristic was observed by Cui and Lundin [30] in the evaluation of pitting immersion performance of the AISI 316L stainless steel weld metal and shown that the preferential corrosion attack occurred in the austenite phase instead of ferrite phase.

4. Conclusions

Based on the experimental results obtained and under the welding conditions used for this study, it is possible to conclude that the dissimilar welding between AWS E309MoL-16 covered electrode and AISI 316L-stainless steel plates resulted in a weld metal microstructure consisting of austenite and δ-ferrite. The morphology varied between vermicular and lathy, characteristic of welds that solidify in the ferrite–austenite mode (FA). It was observed that the dilution does not play a significant role on metallurgical alteration of welds. It was also verified that the heat input used on this work (6, 9 and 12 kJ/cm) does not cause a significant variation on dilution levels. For this reason, the change in chemical composition among the welded plates was not important in order to cause a microstructural change. Otherwise, it was observed that with an increase in welding heat input, due to the variation of the cooling rate, caused a decreasing on δ-ferrite contents and morphology of the weld metals. Conversely, δ-ferrite content influenced the welds hardness values, generating its drop with the reduction of this phase. Regarding the corrosion rate of the weld metal, it was noticed that its value was reduced for higher levels of heat input. This may be attributed to metallurgical changes, especially of δ-ferrite contents, caused by a variation in cooling rate, as mentioned. Strong indicators were compiled to reinforce the theory that the major corrosion phenomenon caused by heavy oils is due to the effect of naphthenic acids.

Acknowledgments

The authors are grateful to ENGESOLDA and LACAM/MEV laboratories of the Universidade Federal do Ceará and to the LEM laboratory of Centro Federal de Educação Tecnológica do Ceará. We are also grateful to LAPROSOLDA of the Universidade Federal de Uberlândia for the ferristoscopy analysis. Brazilian research agencies (CNPq, FINEP e ANP/PRH-31) are also acknowledged for the financial support.

REFERENCES

[1] Bilmes P, González A, Liorente C. Influence of the δ-ferrite solidification morphology of austenitic stainless steel weld metals on joint properties. Weld Res Abroad 1997;43:18 [In Spanish].
[2] Long CJ, DeLong WT. The ferrite content of austenitic stainless steels weld metals. Weld J 1973;52:281.
[3] Lippold JC, Savage WF. Solidification of austenitic stainless steel weldments: part 2 — the effect of alloy composition on ferrite morphology. Weld J 1980;59:48.
[4] Di Schino A, Mecozzi MG, Barteri M, Kenny JM. Solidification mode and residual ferrite in low-Ni austenitic stainless steels. J Mater Sci 2000;35:375.
[5] Inoue H, Koseki T, Ohkita S, Fuji M. Formation mechanism of vermicular and lacy ferrite in austenitic stainless steel weld metals. Sci Technol Weld Join 2000;5:385.
[6] Brooks JA, Yang NCY, Krafcik JS. Clarification on development of skeletal and lathy ferrite morphologies in stainless steel welds. Sci Technol Weld Join 2000;6:412.
[7] Schaeffler AL. Constitution diagram for stainless steel weld metal. Met Prog 1949;56:680.
[8] Delong WT. Ferrite in austenitic stainless steel weld metal. Weld J 1974;53:273.

[9] Kotecki DJ, Siewert TA. WRC-1992 constitution diagram for stainless steel weld metals: a modification of the WRC-1988 diagram. Weld J 1992;71:171.
[10] Kujanpaa VP, David SA, White CL. Formation of hot cracks in austenitic stainless steel welds-solidification cracking. Weld J 1986;65:202.
[11] Radhakrishnan VM. Hot cracking in austenitic stainless steel weld metals. Sci Technol Weld Join 2000;5:40.
[12] Brooks JA, Thompson AW, Williams JC. A fundamental study of the beneficial effect of delta ferrite in reducing weld cracking. Weld J 1984;63:71.
[13] Brooks JA, Thompson AW. Microstructural development and solidification cracking susceptibility of austenitic stainless steel welds. Int Mater Rev 1991;36:16.
[14] ASTM standards. Standard G 1-90, 1-8. Philadelphia, PA: ASTM; 1993.
[15] Folkhard E. Welding metallurgy of stainless steels. New York: Springer-Verlag Wien; 1998.
[16] Elmer JW, Allen SM, Eagar TW. Microstructural development during solidification in stainless steel alloys. Metall Trans A Phys Metall Mater Sci 1989;20A:2106.
[17] Inoue H, Koseki T, Okita S, Fuji M. Solidification and transformation behaviour of austentic stainless steel weld metals solidified as primary ferrite: study of solidification and subsequent transformation of Cr–Ni stainless steel weld metals. Weld Int 1997;11:937.
[18] Brooks JA, Yang N, Krafcik J. Proceedings of "Trends in Welding Science and Technology". Materials Park (Ohio, USA): ASM International; 1992. p. 173.
[19] David SA. Ferrite morphology and variations in ferrite content in austenitic stainless steel welds. Weld J 1981;60:63.
[20] Suutala N, Takalo T, Moisio T. Ferritic–austenitic solidification mode in austenitic stainless steel welds. Metall Trans A Phys Metall Mater Sci 1980;11A:717.
[21] Brooks JA, Williams JC, Thompson AW. Microstructural origin of the skeletal ferrite morphology of austenitic stainless steel welds. Metall Trans A Phys Metall Mater Sci 1983;14A:1271.
[22] A.F. Padilha, L.C. Guedes. (1994). Austenitic stainless steels, Ed. Hemus, São Paulo Brazil. [In Portuguese].
[23] Cardoso RL, Prado EM, Okimoto PC, Paredes RSC, Prokopiak LA. Different CO_2 content shielding gas evaluation on weld-overlay characteristics used in repair of turbine depredated. Sold Insp 2003;11:68 [In Portuguese].
[24] Medvedeva ML. Specifics of high-temperature corrosion processes during oil recovery. Chem Pet Eng 2000;36:749–54.
[25] Silva CC, Machado JPSE, Sobral-Santiago AV, Sant'Ana HB, Farias JP. High-temperature hydrogen sulfide corrosion on the heat-affected zone of the AISI 444 stainless steel caused by Venezuelan Heavy Petroleum. J Pet Sci Eng 2007;59:219–25.
[26] Babaian-Kibala E. Naphthenic acid corrosion in a refinery setting. Proc. Conf. Corrosion 93, New Orleans, LA, USA; March 1993. Paper 631.
[27] Babaian-Kibala E, Nugent MJ. Naphthenic acid corrosion literature survey. Paper n° 378, NACE International, Proceedings, vol. 99. Corrosion; 1999.
[28] Slavcheva E, Shone B, Tumbull A. Review of naphthenic corrosion. Brit Corros J 1999;34:125–31.
[29] Piehl R. Naphthenic acid corrosion in crude distillation units. Mater Perform 1988;44:37.
[30] Cui Y, Lundin CD. Austenite-preferential corrosion attack in 316 austenitic stainless steel weld metals. Mater Des 2007;28:324–8.